Toxicological impact of organic ultrafine particles (UFPs) in human bronchial epithelial BEAS-2B cells at air-liquid interface

Ana Teresa Juarez-Facio, J. Yon, C. Corbière, Tiphaine Rogez-Florent, C. Castilla, H. Lavanant, M. Mignot, C. Devouge-Boyer, C. Logie, Laurence Chevalier, et al.

Toxicological impact of organic ultrafine particles (UFPs) in human bronchial epithelial BEAS-2B cells at air-liquid interface

A. T. Juarez Facio[1], J. Yon[2], C. Corbière[1], T. Rogez-Florent[1], C. Castilla[3], H. Lavanant[3], M. Mignot[3], C. Devouge-Boyer[3], C. Logie[1], L. Chevalier[4], J.-M. Vaugeois[1], C. Monteil[1]

[1] Normandie Univ, UNIROUEN, UNICAEN ABTE, 76000 Rouen, France

[2] Normandie Univ, UNIROUEN, INSA Rouen, CNRS, CORIA, 76000 Rouen, France.

[3] Normandie Univ, INSA Rouen, UMR 6014 CNRS, COBRA, 76801, Saint Etienne Du Rouvray, France

[4] Normandie Univ, UNIROUEN, INSA Rouen, CNRS, GPM-UMR6634, 76000 Rouen, France

*** Corresponding author:** C. Monteil

ABTE-ToxEMAC, UFR Santé, 22 boulevard Gambetta, 76000 ROUEN

+33235148475

E-mail: christelle.monteil@univ-rouen.fr

ABSTRACT

Air pollution has significant health effects worldwide, and airborne particles play a significant role in these effects. Ultrafine particles (UFPs) have an aerodynamic diameter of 0.1 µm or less, can penetrate deep into the respiratory tree, and are more toxic due to their large specific surface area, which should adsorb organic compounds. The aim of this study is to show the toxicological effects of UFPs with high organic content at low dose on BEAS-2B cells through at air-liquid interface (ALI) exposure using a Vitrocell® technology and a miniCAST (Combustion Aerosol Standard) generator. In conjunction with this approach, chemical analysis of particles and gas phase was performed to evaluate the presence of polycyclic aromatic hydrocarbons (PAHs). Chemical analyses confirmed the presence of PAHs in UFPs. With this experimental setup, exposure of the BEAS-2B cells induced neither cytotoxicity nor mitochondrial dysfunction. However, an increase of oxidative stress was observed, as assessed through *Nrf2*, *NQO1*, *HO-1, CuZnSOD, MnSOD,* and *Catalase* gene expression, together with significant induction of genes related to xenobiotic metabolism *CYP1A1* and *CYP1B1.* Negative regulation of inflammatory genes expression (*IL-6* and *IL-8*) was present three hours after the exposition to the UFPs. Taken together, this experimental approach, using repeatable conditions, should help to clarify the mechanisms by which organic UFPs induce toxicological effects.

KEYWORDS: BEAS-2B, Air-Liquid Interface, miniCAST, ultrafine particles, PAH, toxicity

1. INTRODUCTION

The presence of particulate matter in ambient air is responsible of important health impacts in many urban and industrialized zones. Due to its physical properties and health effects, airborne ultrafine particulate matter is getting more attention. Ultrafine particles (UFPs) are defined as particles for which aerodynamic diameter is equal or inferior to 100 nm. The principal sources of UFPs emissions in urban environments are road traffic (mainly caused by Diesel engines) and industrial processes related to energy production, incinerators, construction and home heating (Li et al., 2016; Oberdörster et al., 2005). Despite the very low concentrations of UFPs in the air, they represent very high particle number concentrations. Moreover, because of their higher specific area and surface reactivity, UFPs can adsorb a significant amount of toxic compounds, making them more threatening than larger particulate matter (PM) (Kwon et al., 2020). Therefore, besides morphological characteristics of the particles, their chemical composition also plays an important role in the adverse health effects of UFPs.

UFPs emissions contain a wide range of chemical species in highly variable concentrations depending on the source. For example, traffic emissions include soot particles coated with organic compounds such as alkanes, alkenes, aldehydes, and polycyclic aromatic hydrocarbons (PAHs) surrounded by a gas phase containing CO, CO_2, NO_X, SO_X, VOCs, SVOCs, and water vapor (Kwon et al., 2020). Although it is difficult to disentangle PAHs from other air pollutants derived from combustion processes, they deserve major attention as they are among the key compounds in UFPs toxicity (Kwon et al., 2020; Lee et al., 1995; Walgraeve et al., 2010).

PAHs are organic compounds with two or more fused aromatic (benzene) rings. PAHs with low molecular weight (two or three rings) stay in the vapor phase in the atmosphere, while PAHs with more than three rings are mostly bound to particles allowing them to travel by air and water to soil and sediments, becoming widespread pollutants in the environment. They

are formed during incomplete combustion processes including forest fires, fossil fuels, and wood burning, tobacco smoke, various forms of cooking, industrial processes, and traffic emissions (Hussar et al., 2012). Benzo(a)pyrene (BaP) is the most studied PAHs and is often used as a marker for exposure to carcinogenic PAHs due to its high contribution to the carcinogenic potential (Ohura et al., 2004), that is why the current European directive sets a target value for ambient air concentration of BaP, measured in PM_{10}. However, a broader range of PAH-species may contribute to the health effects of air pollution and may be associated with even smaller particles. Consequently, it is uncertain if the current regulation sufficiently protects against the various health outcomes of PAHs (Lag et al 2020).

UFPs exposure has been implicated in developing of several health outcomes through mechanisms that involve oxidative stress, inflammation, and mitochondrial dysfunction (Araujo and Nel, 2009; Pope and Dockery, 2006; Sotty et al., 2020a). Redox-active organic chemicals on particle surface, as PAHs, are the principal source of reactive oxygen species (ROS) in UFPs (Daiber et al., 2020; Li et al., 2016). A high concentration of these pro-oxidant molecules causes an imbalance between oxidants and antioxidants known as oxidative stress, inducing disruption of redox signaling and molecular damage (Sies and Jones, 2007). The transcription factor Nrf2 is the key regulator to protect cells against the harmful effects of ROS by inducing most of the antioxidants and detoxifications enzymes, as HO-1 and NQO1 (Cho and Kleeberger, 2010). In addition, several proinflammatory signaling pathways are redox-sensitive. Hence, these pathways can be activated and induce airway inflammation after a failure of cells to restore redox homeostasis (Araujo and Nel, 2009; Biswas and Rahman, 2009). Inflammation is characterized by the activation of several signaling pathways in response to stress. The inflammatory response involves both anti- and pro-inflammatory mediators shown by the expression of cytokines and transcription factors (Chen et al., 2017). Along with oxidative stress and inflammation, mitochondrial dysfunction has been reported to be a mechanism induced by airborne PM. Mitochondria play a crucial role in cellular

bioenergetics by the synthesis of adenosine triphosphate (ATP), and they are also important regulators of oxidative stress through the generation of ROS (Lavrich et al., 2018; Wang and Tang, 2018). The mentioned pathways may be initiated by PAHs binding to the aryl hydrocarbon receptor (AhR) (Låg et al., 2020), resulting in up-regulation of AhR-regulated genes as CYP enzymes (Nebert et al., 2004). However, although there have been many of studies on the toxicity of PM, there are few studies specific to UFPs, and several uncertainties remain to be clarified, such as the specific toxicological effects observed after UFPs exposures and the contribution of PAHs in these cellular effects.

Many toxicological studies have been performed with PM collected *in-situ* (Bengalli et al., 2019, 2017; Borgie et al., 2015; Cho et al., 2018). This approach is relevant to examine toxicity associated with a specific site and/or season. However, the collected particles are suspended in a liquid medium for subsequent contact with cells, which may induce potential shortcomings, such as the loss of volatile organic compounds and microphysical properties of UFPs. Moreover, *in vitro* assessments in submerged conditions are not representative of physiological conditions where the layer of lung-lining fluid that covers cells is very thin (Blank et al., 2006). Thus, exposure at ALI depicts a better evaluation of exposure by inhalation (Bérubé et al., 2010; Bhowmick and Gappa-Fahlenkamp, 2016).

In this context, following our previous *in vitro* work on the toxicity of combustion-derived particles (Juarez-Facio et al., 2022), the objective of this study is to provide a description of this *in vitro* methodological approach and investigate the potential toxicity mechanisms involved after PAHs-rich UFPs exposures at low dose. A Combustion Aerosol Standard aerosol (mini-CAST) generator was used with a selected operational condition in order to produce UFPs with a high content in PAHs. The miniCAST was directly connected to a Vitrocell® System for *in vitro* exposures at air-liquid interface (ALI). Particle and gaseous phases were chemically characterized. *In vitro* assessment was performed with the cell line

Beas-2B, which has a high capacity of PAHs metabolization (Uppstad et al., 2010), and different biological responses related to oxidative stress, inflammation, xenobiotic metabolism, and mitochondrial function were investigated. This approach allows studying in a reproducible manner toxicity PAHs-rich UFPs, without potential confounding factors like variations in air quality, metals or other compounds present in field samples and keeping the properties of the aerosol.

2. MATERIALS AND METHODS

2.1. Chemicals

Unless otherwise specified, chemicals were purchased from Sigma-Aldrich (St Quentin Fallavier, France).

2.2. Exposure system

The exposure system consisted of a soot generator miniCAST (5201c), a Vitrocell® exposure system, and several devices for physical characterization and sampling points for chemical analysis, as previously described (Juarez-Facio et al., 2022). A schematic of the experimental setup is shown in **Figure S1**. The studied aerosol was chosen for its high content in organic carbon and for assuring modal diameter lower than 100 nm. The operating condition in miniCAST consisted of propane combustion controlled with different flow rates: propane (60 mL/min), nitrogen (7 mL/min), oxidation air (1 mL/min), and dilution air (20 L/min).

2.3. Aerosol characterization

Mass concentration was measured with a Tapered Element Oscillating Microbalance (TEOM) and controlled with the Pegasor Particle Sensor (PPS–M PEGASOR). Number and particle size distributions were measured with a Scanning Mobility Particle Sizer (SMPS – DMA 3082 – CPC 3756) downstream of the Vitrocell® system. To examine particle morphology, soot particles were deposited onto a grid (200-mesh copper grid with a Formvar/carbon film, Agar Scientific) and then observed with a high-resolution microscope (JEOL, JEM-3010 model) using transmission electron microscopy (TEM). The chemical characterization focused on both the gas phase and soot is described in the supplementary experimental part.

Dose exposure was determined in two steps. First, deposited mass rate was measured by the quartz crystal microbalance (QCM – Vitrocell®) integrated into the exposure module. Then,

deposition factor is increased by activating the electrostatic precipitator for which enhancement factor was determined with the Scanning Mobility Particle Sizer (SMPS): Aerosol size distributions were measured, upstream and downstream of the exposure module, with and without an electric field. The exposure dose was estimated to be 1775.0 ng/cm² deposited in 35 min, at a flow rate of 10 mL/min/well as described below. This exposure dose was chosen according to previous results (Juarez-Facio et al., 2022).

2.4. Cell culture and exposure conditions

BEAS-2B cell line (ATCC – CRL9609™) derived from normal human bronchial epithelial cells were obtained from an autopsy of non-cancerous individuals. BEAS-2B cell line was cultured in LHC-9 medium (GIBCO) supplemented with 10 U/ml penicillin and 10 µg/ml streptomycin in collagen pre-coated flasks to improve cell adherence until 75-80% of confluence. Then, they were seeded at a density of 90,000 cells per cm^2 on collagen-coated Transwell™ inserts. Culture was maintained in liquid-liquid interface for 10 days prior to exposure. Then, the apical medium was removed, and air-liquid interface was carried out during and after exposure. The cultures were maintained in 95% humidified air with 5% CO_2 at 37°C.

During exposure, cells were placed in the Vitrocell® system and exposed at air-liquid interface (ALI) to aerosol (exposure module) or to HEPA-filtered clean air (air control module) for 35 minutes. Aerosol was delivered to each well by isokinetic sampling at a 10 mL/min/well flow rate. Each module was designed for simultaneous exposure of three independent replicates. An electrical field (+1000 V) was used to increase particles deposition. Cellular response relative to control was then evaluated, 3 h and 24 h following the exposure.

2.5. Biological endpoints

2.5.1 Cell viability

Cell viability after exposure was assessed using the MTT assay (formazan product formed by functional mitochondrial dehydrogenases). After 3 h and 24 h exposure, inserts were rinsed with phosphate-buffered saline (PBS-1X). Then, 0.05 mL of MTT solution (50 µg/mL) was added in 0.5 mL of LHC-9 medium to the lower chamber for 3 h. To dissolved formazan crystals, 0.8 mL of SDS (10% in 0.1 N HCl) were added to lower and upper chambers and incubated during the night. The extracted solution was transferred to 96 well plates, and absorbance was measured at 570 nm (Xenius, Safas, Monaco). Results were calculated with the absorbance of the samples normalized to the control, which was set to 100%.

2.5.2 Gene expression

Total RNAs were isolated using Direct-zol™ RNA MiniPrep (Ozyme) according to the manufacturer's instructions. RNA concentration and purity were measured with a NanoDrop spectrophotometer (NanoDrop™ 2000 / 2000c.). RNA integrity numbers of the samples were > 8. DNase treatment was carried out with DNase I, Amplification Grade (Invitrogen™). cDNAs were synthesized using Invitrogen™ Transcriptase inverse (M-MLV) from 1 µg of total RNA. Real-time PCR was performed with the cDNA samples and Brilliant III Ultra-fast SYBR Green QPCR Master Mix on Stratagene Mx3005P System (Agilent Technologies). Expression profiles of *Nrf2, NQO1, HO-1, CuZnSOD, MnSOD, Catalase, IL-6, IL-8, CYP1B1,* and *CYP1A1* were normalized to *B2M*. Primers sequences are shown in **Table S2**. Results are expressed as relative expression using the $2^{-\Delta\Delta Ct}$ method (Livak and Schmittgen, 2001).

2.5.3 Assessment of oxygen consumption

Oxygen consumption was assessed with the Seahorse XF HS mini analyzer (Agilent Technologies, les Ulis, France) from cells exposed 24 h to particles, after 3 days on culture at

ALI. After the exposures, cells were harvested and replated in XFp8 miniplates (Agilent Technologies) at 30000 cells/well. 24 h later, oxygen consumption rates (OCR) were measured according to the manufacturer's instructions. Briefly, cells were washed once with XF DMEM media (Agilent) supplemented with 1 mM pyruvate, 2 mM glutamine, and 10 mM glucose at pH 7.4. Then, cells in DMEM were incubated for 1 h at 37 °C in non-CO_2 incubator. Measurements of baseline OCR were determined before administration of different drugs of the assay (Mitochondrial stress test – Agilent Technologies). Next, media was removed, and cells were frozen until the determination of protein content. OCR were normalized against protein content and data analysis was conducted with the Seahorse Wave software (Agilent Technologies).

2.5.4 ATP and ADP measurements

After 3 h and 24 h exposure, inserts were washed in PBS-1X and incubated in 500 µL of perchloric acid solution (1 N) for 60 minutes at 4 °C. Cells were subsequently harvested by scraping and centrifuged at 13500 g for 5 minutes at 4 °C. Pellets were resuspended in NaOH (1 N) and used to determine proteins concentration by Lowry assay. Supernatants were neutralized by the addition of K_2CO_3 (2 M) and centrifuged at 13500 g for 5 minutes at 4 °C. Supernatant was collected and stored at -80°C until use.

Intracellular ATP and ADP amounts were quantified by high performance liquid chromatography coupled with a diode array detector (HPLC-DAD, 1260 Infinity II, Agilent Technologies). Analytes were separated on a Poroshell 120 EC-C18 (3 x 150 mm, 2.7 µm) with guard EC-C18 (3 mm). Briefly, 10 mM ATP and ADP stock solutions were prepared by dissolving the appropriate amounts in ultrapure water. The above stock solutions were all stored at -20 °C; the working solutions were prepared daily by appropriate dilution in the mobile phase. The mobile phase consisted of 50 mM of potassium hydrogen phosphate (pH 6.80). The chromatographic separation was carried out at 20 °C with 0.6 mL/min as flow rate. The

identification of peaks was based on comparing retention times and diode-array spectra of chemicals standard and biological samples. For the quantification, the UV data were collected at 254 nm. The analytical method was validated by assessing the linearity, limits of quantification and detection, and accuracy to meet the ICH requirements.

2.5.5 Total glutathione measurement (GSH)

Total glutathione measurements were performed with supernatants obtained for ATP and ADP quantification. Briefly, 40 µl of the sample, 200 µl of reagent pad, and 40 µl of glutathione reductase (8.5 U/mL) were deposed in a 96 well plate, and absorbance was measured at 405 nm for 2 min and 40 s. The reagent mix consisted of NADPH (0.4 mM), DTNB (1 mM) and methanol (10%) (VWR, Fontenay-sous-Bois, France) in buffer (160 mM $Na_2H_2PO_4$; 8 mM EDTA, pH 7.4). GSH levels were determined from a standard curve and normalized to the corresponding well's protein content (Lowry assay).

2.5.6 Statistical analysis

At least three independent experiments were performed, in duplicate for each biological endpoint, and results were expressed as mean ± SD. Statistical analysis was performed using the non-parametric Mann-Whitney U-test (GraphPad for Windows, v9.0). Statistically significant differences were reported with $p < 0.05$.

3. RESULTS

3.1. Aerosol characterization

During exposure, mass concentration was 57.85 mg/m^3, geometric median (GM) mobility diameter was 58.9 ± 1.53 nm, and total count concentration was 1.63E+08 N/cm^3. These measures correspond to the particle conditions delivered to cells. Size distribution by SMPS and transmission electron microscopy image are reported in **Figure 1**.

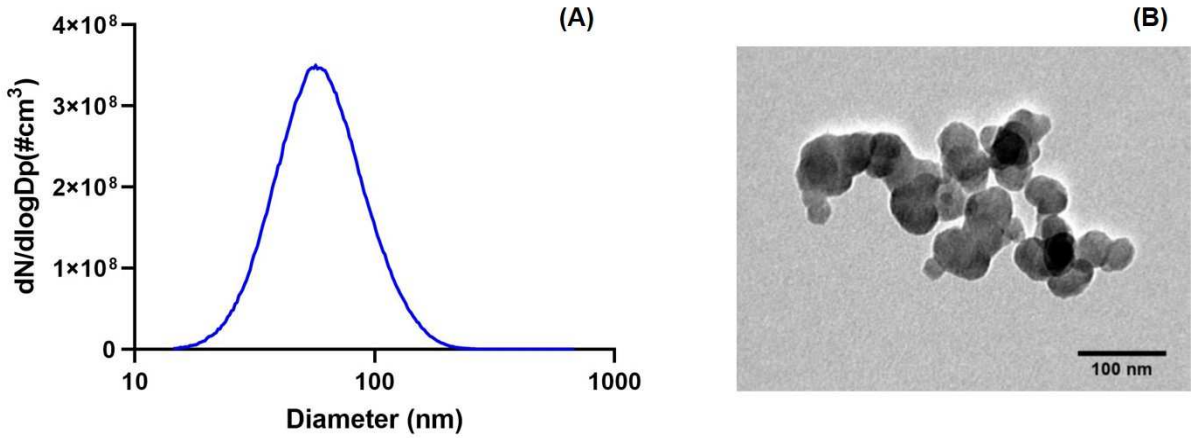

Figure 1: (A) Size distribution by SMPS and (B) Transmission electron microscopy image of particles

A typical mass spectrum of the organic aerosol sample using laser desorption ionization (LDI) with ultra-high-resolution mass spectrometry (FT-ICR MS) is shown in **Figure 2**. The main distribution of ions was observed between *m/z* 200 and *m/z* 900 and centered around *m/z* 400. This distribution was easily resolved with FTICR and few isobaric compounds were found within each nominal mass. The mass precision of the FTICR led to the reliable attribution of 1800 molecular formulas, with 85-90% common to all the replicates, as shown in the Venn diagram of **Figure S2**. Hydrocarbons and molecules with one and two oxygen atoms were mostly found in the sample, as shown in the insert in **Figure 2** representing ion relative intensities for each molecular class.

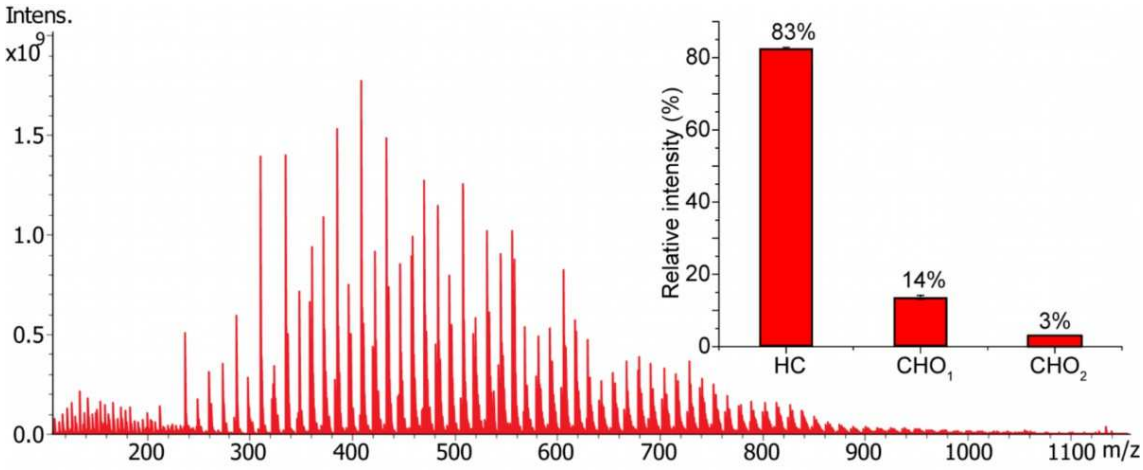

Figure 2: LDI (+) FTICR mass spectra of organic aerosol sample. The insert corresponds to the relative intensity of the main three molecular class observed within the sample: hydrocarbons (HC), and hydrocarbons with one (CHO_1) and two (CHO_2) oxygen atoms.

The **Figure 3** shows the diagram of the double bond equivalent (DBE) *vs* carbon number for hydrocarbons. DBE, also called degree of unsaturation or index of hydrogen deficiency totals the number of rings and π bonds present in a molecule. For ions, DBE values can be either integer or half-integer numbers depending on the type of ion: $M^{+\cdot}$ (with an odd number of electrons and an even nominal mass) or $[M + H]^+$ and $[M - H]^+$ (with an even number of electrons and an odd nominal mass). Both types of ions can be obtained from LDI depending on molecule's ionization energy and gas-phase basicity.

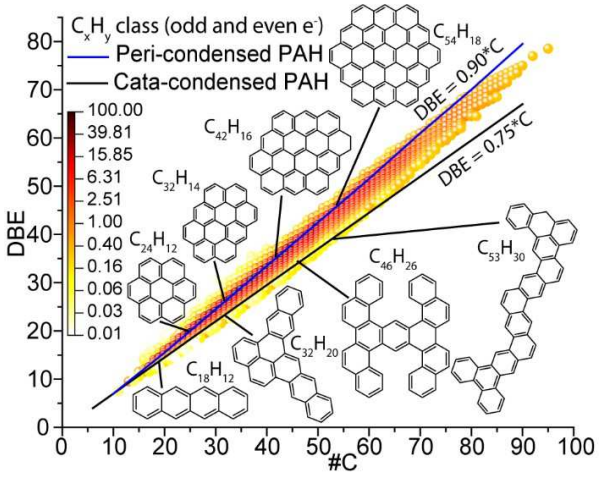

Figure 3 : DBE vs #C diagrams of LDI FTICR MS data from the CAST sample for hydrocarbon compounds with odd and even number of electrons. The colors indicate the relative intensity of the ions. The lower black line represents the trend of cata-condensed PAH, and the upper blue line

represents the trend of peri-condensed PAH. Putative neutral structures found in the sample were added.

A single distribution of ions was observed for the molecular class chosen with a number of carbon atoms between 10 and 100, and DBE values between 10 and 80 (**Figure 3**). These DBE values were very high and corresponded to highly aromatic compounds. Two lines were drawn in the diagram, corresponding to two limits of PAH structures: the cata-condensed and peri-condensed PAH, described in many studies (Hsu et al., 2011; Jacobson et al., 2020; Siegmann and Sattler, 1999). The cata-condensed structures have no carbon atoms shared by more than two aromatic rings and have a $C_{(4i+2)}H_{(2i+4)}$ formula. The peri-condensed PAH have their carbons shared with more than two aromatic rings. Their formulas obey the relationship by K. Siegmann et al. (Siegmann et al., 1995) in **equation 1**.

$$[Carbon\ number] = \frac{[Hydrogen\ number]^2}{6} \quad (1)$$

The peri-condensed and cata-condensed PAH lines were drawn using the equations showed in **Table S2**. As shown in **Figure 3**, most of the ions observed in LDI FTICR MS were above the cata-condensed curve, and most of the highest intensity ions (**Table S3**) followed the peri-condensed PAH line, indicating that highly condensed PAH were generated during the experiment. Similar characteristics were observed for the molecular class containing one oxygen atom (**Figure S3).**

Concerning the gaseous phase, the main compounds, presented in **Table S5**, were carbon dioxide (0.6%), dihydrogen (0.04%), acetylene (0.03%), methane (0.02%), ethylene (0.01%), propyne (0.0007%), propadiene (0.0006%). Other compounds (i.e., propene, propane, 1-buten-3-yne, 1,3 butadiyne, benzene) were detected but at levels under the LQ.

3.2. Cell viability after clean air exposure

To validate the applicability of BEAS-2B cells in ALI for exposure experiments, we first performed a viability study at 3 h and 24 h after 35 min of exposure to clean filtered air (Air control) using the Vitrocell ® system, compared to cultures left in the incubator (Incubator). Next, we evaluated cell viability by the MTT test (**Figure 4**). A slight but not significant reduction of viability was reported compared to incubator controls at 3 h and 24 h after exposure. Based on these results, control air was chosen as a control for particle exposure analysis.

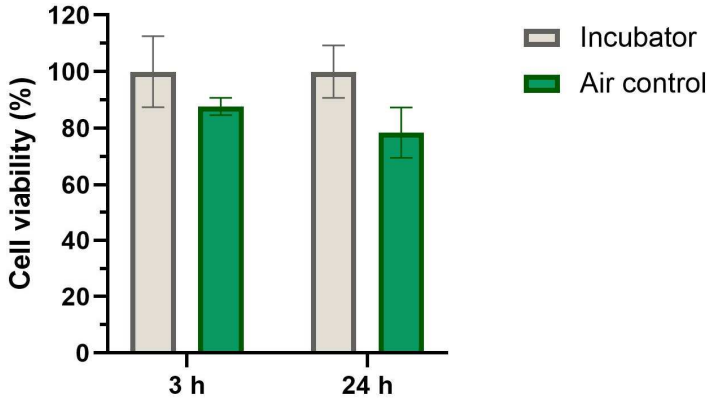

Figure 2: Cell viability by MTT test (as a percent of incubator) in BEAS-2B cells in response to clean air exposure for 35 minutes in the Vitrocell system. Data were expressed as mean ± SD of 3 independent experiments

3.3 Cellular response after aerosol exposure

3.3.1. Cell viability

Then, BEAS-2B cells were exposed to the aerosols for 35 min resulting in the deposition of approximately 1.8 µg/cm^2. Cell viability was evaluated after 3 h and 24 h and compared to control air. The cells maintained good viability, as observed either with the MTT test or with the ATP/ADP ratio (**Figure 5**).

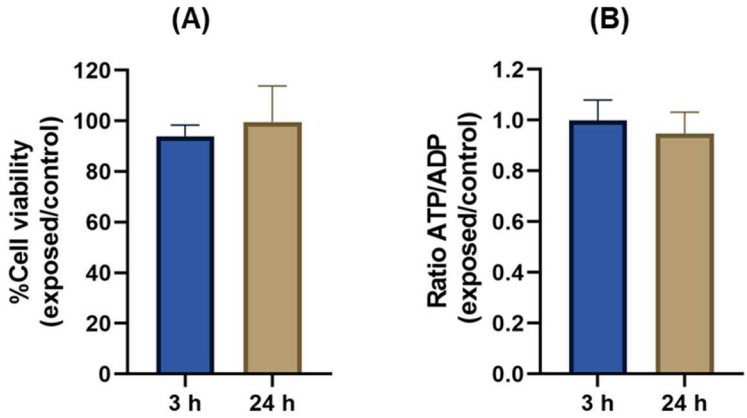

Figure 3: (A) Cell viability determined by MTT assay and (B) ATP/ADP ratio measurement by HPLC 3 h and 24 h after exposure of organic UFPs. Data were expressed as mean ± SD of 3-4 independent experiments.

These results follow those observed after measuring the mitochondrial function, analyzed using the Cell Mito Stress test (**Figure 6**). During this test, the cells were sequentially exposed to oligomycin, an ATP synthase inhibitor, carbonyl cyanide-4-(trifluoromethox) phenylhydrazone (FCCP), an uncoupler, and rotenone with antimycin A, two chain inhibitors. The OCR measured in these conditions evaluated non-mitochondrial and basal respiration, proton leak, ATP production, and spare respiratory capacity. All these parameters were unaffected in our experimental conditions. These results were obtained 24 h after exposure to particles since the Seahorse technology used in the present study requires replating cells in the Seahorse miniplates, and in submerged conditions, one day prior to assay.

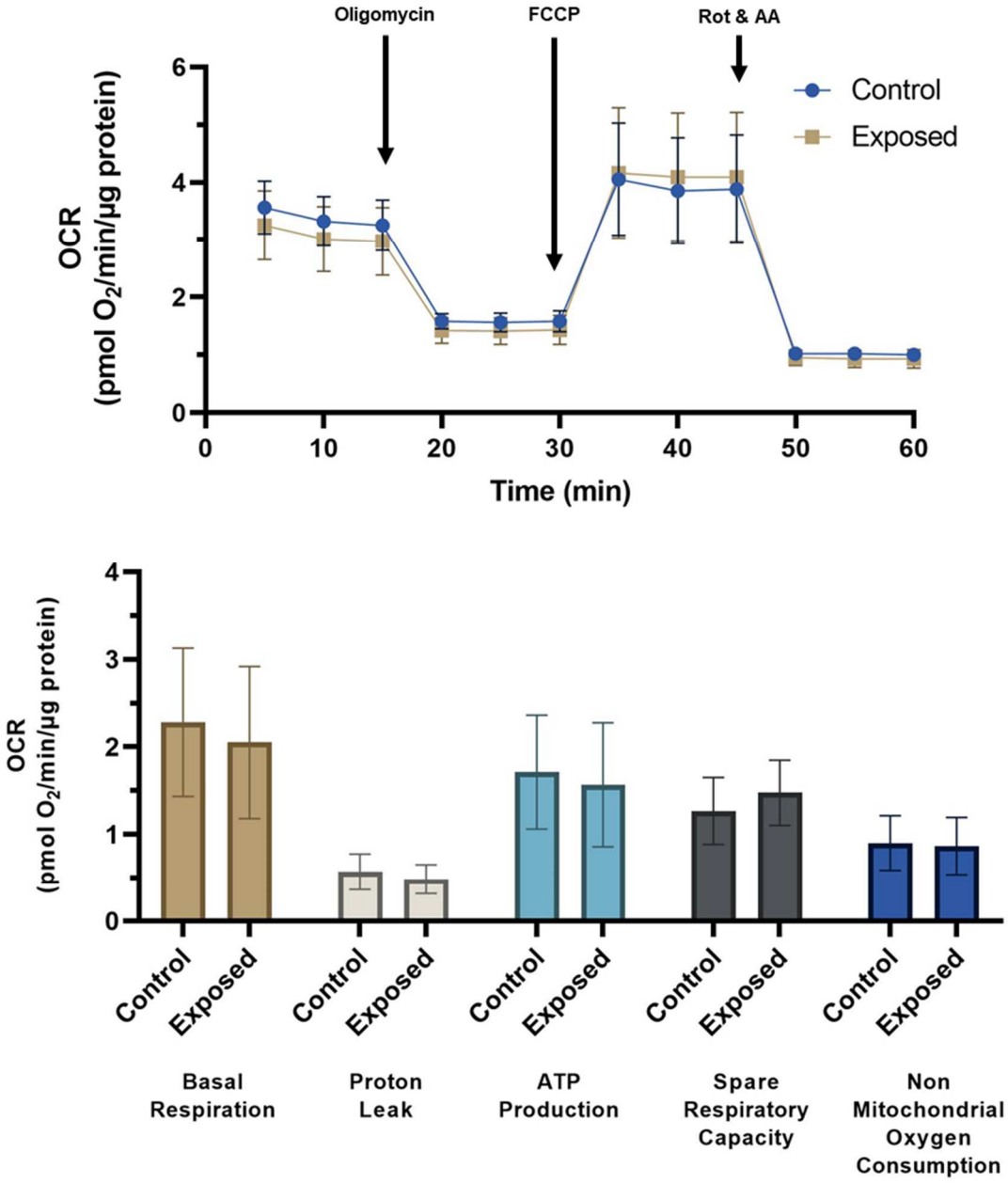

Figure 4: Oxygen consumption rates (OCR) in human bronchial epithelial BEAS-2B cells exposed to UFPs or filtered air. Results were expressed as mean ± SD of 4 independent experiments.

3.3.2 Oxidative stress and inflammation parameters

As shown in **Figure 7**, significant up or downregulation of oxidative stress markers genes was measured in BEAS-2B cells after particles exposure compared to air control (*p<0.05* and *p<0.005*). In this work, *Nrf2* was slightly upregulated 24 h after exposure (**Figure 7A**). In order

to study the Nrf2 signaling pathway activation, we studied the expression of two Nrf2 target genes, *NQO1 and HO-1. NQO1* was slightly but significantly upregulated in both time conditions (**Figure 7B**), while *HO-1* was almost 4 times upregulated at 3 h but then gets back to the control ratio at 24 h (**Figure 7C**). Furthermore, *CuZnSOD* was slightly but significantly upregulated at 24 h (**Figure 7D**), contrary to *MnSOD*, which was downregulated at 3 h (**Figure 7E**). *Catalase* was not significantly changed at any condition (**Figure 7F**).

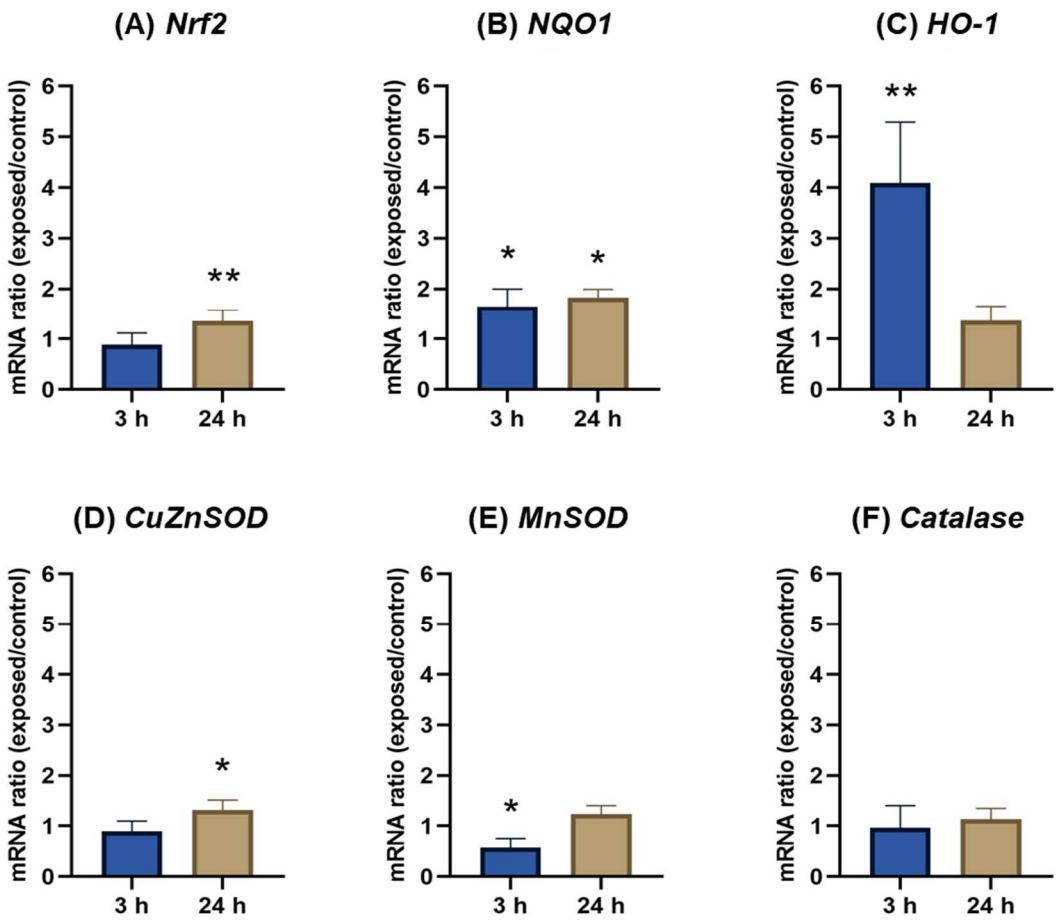

Figure 5: Gene expression in BEAS-2B cells exposed to UFPs. Cells were exposed to organic aerosol (+1000V) for 35 min and incubated with particles for 3 h and 24 h. Results were expressed as mean ± SD of 4 independent experiments. Statistically significant differences were reported with $p < 0.05$

Along with the oxidative response, total glutathione was measured using a colorimetric protocol (**Figure 8**). The levels were significantly reduced after 3 h exposure followed by an increase after 24 h, compared to air control.

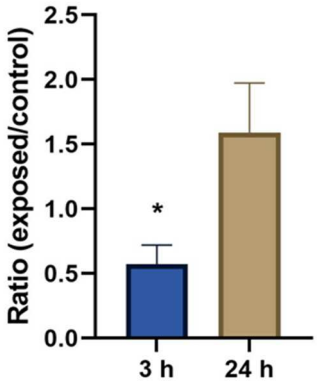

Figure 6: Total glutathione levels in BEAS-2B cells exposed to UFPs. Cells were exposed to organic aerosol (+1000V) for 35 min and incubated with particles for 3 h and 24 h. Results were expressed as mean ± SD of 4 independent experiments. Statistically significant differences were reported with $p < 0.05$

Inflammation markers, *IL-6* and *IL-8,* were downregulated only after 3 h exposure compared to air control (**Figure 9**).

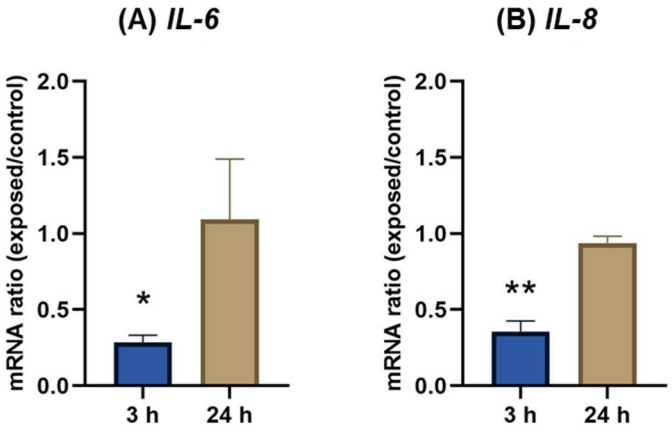

Figure 7: Gene expression in BEAS-2B cells exposed to UFPs. Cells were exposed to organic aerosol (+1000V) for 35 min and incubated with particles for 3 h and 24 h. Results were expressed as mean ± SD of 4 independent experiments. Statistically significant differences were reported with $p < 0.05$

3.3.3 Expression of genes related to xenobiotic metabolism

Gene expression of metabolizing enzymes was highly upregulated at both time conditions (**Figure 10**). *CYP1B1* was 2.5 and 4 times over-expressed, while *CYP1A1* was upregulated 17- and 18-times compared to air control, after 3 h or 24 h of exposures, respectively.

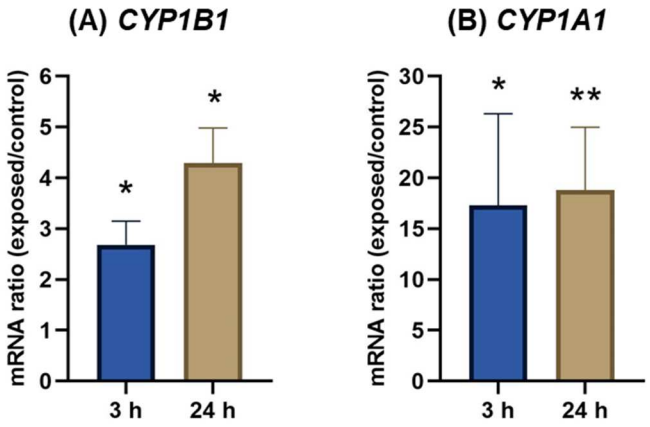

Figure 8: Gene expression in BEAS-2B cells exposed to organic aerosol. Cells were exposed to organic aerosol (+1000V) for 35 min and incubated with particles for 3 h and 24 h. Results were expressed as mean ± SD of 4 independent experiments. Statistically significant differences were reported with $p < 0.05$

4. DISCUSSION

This study described a novel methodological approach to study biological effects of aerosols containing a low dose of PAHs-rich ultrafine particles, using BEAS-2B cells at ALI and exposed with an online exposure device. Using different endpoints associated to oxidative stress, xenobiotic metabolism and mitochondrial function, the greatest responses appeared on the expression of genes related to the metabolism of xenobiotics.

We focused in this study on PAHs-rich UFPs characterized by a mobility diameter of 58.9 ± 1.53 nm, with a high content in organic compounds (OC/TC: 87 ± 5 %), as previously described (Bescond et al., 2016). The dimensions of these particles agree with those of soot particles from various sources, such as diesel particles (Hawley et al., 2014) or biomass burning (Longhin et al., 2016). In this study, the non-targeted analysis identifies a wide range of PAHs as seen on the DBE vs #C plot, which is a powerful tool for the characterization of complex matrices and the comparison of samples. The observed compounds were highly aromatic compounds, such as PAHs and oxy-PAHs, which are readily ionizable within the LDI source. The presence of oxygenated species corresponds to the insertion of oxygen atoms by the air used for the combustion experiment. The very low levels of gaseous compounds analyzed by GC/TCD and GC/MS, and the short-term exposure applied in this study to the cells (35 min) indicate that the observed biological responses can be only attributable to UFPs and their associated PAHs.

In this study, the BEAS-2B cell line was grown on transwell inserts 10 days before aerosol exposure. To our knowledge, very few studies have used this approach for studying UFPs. Similar cultured conditions were previously studied, where BEAS-2B cells were cultured towards a differentiated phenotype (Stewart et al., 2012). At ALI conditions, these cells were reported to express β-tubulin IV and showed localized ZO-1 and E-Cadherin staining. Compared to primary models, line cell models presented less variability between passages

and experiments (Stewart et al., 2012). Moreover, these cells are metabolically active (Uppstad et al., 2010), and a previous study demonstrated their ability to take up PAHs associated with UFPs (Penn et al., 2005). Therefore, BEAS-2B cells represent an appropriate model to study the toxicity of inhaled UFPs. Our study used this cellular model for exposures online to aerosols in the Vitrocell® system after checking cell viability. Clean air exposure reduced cell viability, as previously reported with clean air at 2 and 8 mL/min flow rates for 3 hours, due to desiccation of the exposed cells (Mistry et al., 2020). Although we used a great flow rate, our time of exposure was short (35 min), to limit this effect. This time was sufficient to obtain a delivery dose at 1.8 µg/cm^2, which was among the lowest reported in the literature (Leclercq et al., 2018a; Sotty et al., 2020b). In these experimental conditions, MTT assay and ATP levels supported the absence of cytotoxicity after both 3 h and 24 h of exposure to particles. Concerning the energy metabolism of the cells, we further examined mitochondrial function using the Seahorse Extracellular Flux Analyzer and confirmed the absence of effect on cellular metabolism. However, a limitation of this approach was the use of submerged conditions and seeding cells one day prior to the reading that could explain this result. Other experiments are needed to confirm this observation, using a more appropriate approach to monitor the cellular metabolism of ALI epithelial cells, as recently described by Mavin et al., 2020 (Mavin et al., 2020).

Overall, several biological markers were significantly altered under these non-cytotoxic conditions and without observed cellular metabolism alteration. GSH levels were significantly reduced after 3 h exposure, followed by an increase after 24 h, as compared to control. GSH is the principal antioxidant in the lung and its depletion has been observed after acute cigarette smoke (CS) exposure. In contrast, prolonged exposure to CS induces a GSH increase due to upregulation of the expression and activity of enzymes involved in GSH production (Dalle-Donne et al., 2020). It has also been demonstrated that increased cellular levels of glutathione are necessary for tumor initiation and proliferation (Harris et al., 2015). Our results may reflect

early oxidative stress, which may play an important role in the initiation and progression of chronic pathologies, although complementary experiments are needed. This hypothesis is reinforced by the induction of HO-1, a cytoprotective enzyme, 3 h after exposure. Induction of HO-1 associated to GSH depletion has been shown in lung fibroblasts after CS exposure (Baglole et al., 2008) and in BEAS-2B cells after UFPs exposure (Li et al., 2003). In this last study, the authors observed a correlation between the high organic carbon and PAHs contents of UFPs and HO-1 expression, suggesting a role of organic agents in generating redox activity (Li et al., 2003). Interestingly, the expression of CYP1B1 and CYP1A1 were significantly increased in our study, at both time conditions. Organic compounds as PAHs can explain these results, as they can induce cytochrome P450 metabolic enzymes. CYP1A1 is highly inducible by PAH and, as CYP1B1, plays an important role in PAH metabolism about carcinogenesis, due to the formation of oxidized metabolites (Moorthy et al., 2015). These metabolites were further metabolized to more polar and detoxified products by phase II enzymes, such as NQO1. In our experimental conditions, we found a modest upregulation of NQO1, an enzyme which exerts cytoprotective, antioxidant, and anti-inflammatory effects in the lungs (Rubio et al., 2011). *Nrf2* regulates both *HO-1* and *NQO1*. The transcription factor *Nrf2* gene is known to have an important role in resistance to oxidative stress (Ma, 2013). Surprisingly, this gene was upregulated only after 24 h of exposure. This response could be related to Nrf2 degradation in cells under stress, as it has been previously shown by Leclercq et al. 2018. (Leclercq et al., 2018b). We also found that copper-zinc-superoxide dismutase expression (*CuZnSOD*) was slightly up-regulated 24 h following exposure while manganese superoxide dismutase (*MnSOD*) expression was reduced 3 h following exposure to organic UFPs. Catalase expression kept stable following exposure. *CuZnSOD*, *MnSOD,* and *catalase* are antioxidant defense enzymes, and SODs catalyzed the redox transformation of superoxide into oxygen and hydrogen peroxide. The detoxification process is followed by converting hydrogen peroxide to water and oxygen by catalase and other enzymes as glutathione peroxidases

(Fukai and Ushio-Fukai, 2011; Palma et al., 2020). MnSOD plays an important role in neutralizing superoxide in the mitochondrial matrix (Hernandez-Saavedra et al., 2017). A decrease in MnSOD expression induced by PAHs-rich UFPs may contribute to an increase in superoxide levels. Similar results have been reported by Cui et al. 2020 (Cui et al., 2020). In this study, MnSOD expression was notably reduced on lymphatic endothelial cells after exposure to $PM_{2.5}$ (Cui et al., 2020).

Concerning inflammatory markers, contrary to most *in vitro* studies of UFPs (Fuentes-Mattei et al., 2010; Totlandsdal et al., 2015, 2012) and our previous study (Juarez-Facio et al., 2022), we reported a down regulation of IL-8 and IL-6, 3 h following exposure. Interestingly, a recent study showed a down-regulation of IL-6 expression in BEAS-2B cells exposed to particulate matter emissions from gasoline fuels with varying aromatic and ethanol levels (Ahmed et al., 2020). In this study, aromatics content contributed to significant PAHs-mediated IL-6 downregulation. Therefore, it is possible that the negative regulation of inflammatory responses induced by fuels with varying aromatic and ethanol levels is linked to PAHs and their derivatives in the PM emissions (Ahmed et al., 2020). Interestingly, a decrease in IL-8 levels has been previously observed after exposure to volatile organic compounds and PM2.5 (Audi et al., 2017). Inhibition of IL-8 secretion in Calu-3 cells exposed to airborne particulate matter was also reported by (Alfaro-Moreno et al., 2009). Hence, the relationship between PAHs and pro-inflammatory mediators is still unclear.

Overall, our study suggests that organic UFPs elicit an important cellular alteration. Antioxidant and inflammatory responses were observed principally 3 h after exposure, and the greatest response is related to xenobiotic metabolism at both time conditions. However, this study had some limitations that should be addressed. The results are only based on transcriptional observations and have not been validated at the protein levels. Thus, future confirmatory analyses are needed to ascertain the relevance of the variation of gene expressions observed

herein, principally xenobiotic metabolism enzymes genes. Particularly future studies should investigate whether the significant decreases of gene expression of IL-6 and IL-8 after 3 h of exposure will also be observed at the protein expression and secretion levels. Positive control for oxidative stress and inflammation in BEAS-2B cells was not included in the present study and, although there is strongly supporting evidence in the literature that BEAS-2B cells can induce such reactions when comparable methods are used (Badran et al., 2020; Boots et al., 2012; Dergham et al., 2012; Liu and Meng, 2018; Ricciardolo et al., 2012; Xin et al., 2019), this should be investigated in a future work.

5. CONCLUSION

This study presents a methodological approach to evaluate the impact of freshly emitted organic UFPs originating from a controlled setup. For the UFPs emitted by the soot generator miniCAST, our results showed that, although no cytotoxicity nor ATP alterations were observed, the organic UFPs induced an antioxidant response and a negative regulation of inflammatory response as well as induction of xenobiotic-metabolizing enzymes. To further this study, repeated exposures would be interesting as BEAS-2B cells represent a relevant model. Furthermore, our approach may allow scrutinizing the kinetics of inflammatory response. This approach should contribute to elucidate the role of the PM-adsorbed organic components in causing lung injuries. Moreover, the present protocol could be used to study other kinds of particles or other fuels.

6. ACKNOWLEDGMENTS

This work was supported by ANSES (French Agency for Food, Environmental and Occupational Health and Safety; PNREST ANSES EST/2017/1/190), the Regional Council of Normandy and the European Union in the framework of the ERDF-ESF (CellSTEM project) and the Laboratoire d'Excellence (LabEx) SynOrg (ANR-11-LABX-0029). A. T. Juarez Facio received a PhD fellowship funded by ADEME (Agency for Ecological Transition). We gratefully acknowledge Agilent Technologies for lending the Seahorse Xfp Analyzer.

REFERENCES

Ahmed, C.M.S., Yang, J., Chen, J.Y., Jiang, H., Cullen, C., Karavalakis, G., Lin, Y.-H., 2020. Toxicological responses in human airway epithelial cells (BEAS-2B) exposed to particulate matter emissions from gasoline fuels with varying aromatic and ethanol levels. Sci Total Environ 706, 135732. https://doi.org/10.1016/j.scitotenv.2019.135732

Alfaro-Moreno, E., Torres, V., Miranda, J., Martínez, L., García-Cuellar, C., Nawrot, T.S., Vanaudenaerde, B., Hoet, P., Ramírez-López, P., Rosas, I., Nemery, B., Osornio-Vargas, A.R., 2009. Induction of IL-6 and inhibition of IL-8 secretion in the human airway cell line Calu-3 by urban particulate matter collected with a modified method of PM sampling. Environ Res 109, 528–535. https://doi.org/10.1016/j.envres.2009.02.010

Araujo, J.A., Nel, A.E., 2009. Particulate matter and atherosclerosis: role of particle size, composition and oxidative stress. Part Fibre Toxicol 6, 24. https://doi.org/10.1186/1743-8977-6-24

Audi, C., Baïz, N., Maesano, C.N., Ramousse, O., Reboulleau, D., Magnan, A., Caillaud, D., Annesi-Maesano, I., 2017. Serum cytokine levels related to exposure to volatile organic compounds and PM2.5 in dwellings and workplaces in French farmers - a mechanism to explain nonsmoking COPD. Int J Chron Obstruct Pulmon Dis 12, 1363–1374. https://doi.org/10.2147/COPD.S117866

Badran, G., Verdin, A., Grare, C., Abbas, I., Achour, D., Ledoux, F., Roumie, M., Cazier, F., Courcot, D., Lo Guidice, J.-M., Garçon, G., 2020. Toxicological appraisal of the chemical fractions of ambient fine (PM2.5-0.3) and quasi-ultrafine (PM0.3) particles in human bronchial epithelial BEAS-2B cells. Environ Pollut 263, 114620. https://doi.org/10.1016/j.envpol.2020.114620

Baglole, C.J., Sime, P.J., Phipps, R.P., 2008. Cigarette smoke-induced expression of heme oxygenase-1 in human lung fibroblasts is regulated by intracellular glutathione. Am J Physiol Lung Cell Mol Physiol 295, L624-636. https://doi.org/10.1152/ajplung.90215.2008

Barrère, C., Hubert-Roux, M., Lange, C.M., Rejaibi, M., Kebir, N., Désilles, N., Lecamp, L., Burel, F., Loutelier-Bourhis, C., 2012. Solvent-based and solvent-free characterization of low solubility and low molecular weight polyamides by mass spectrometry: a complementary approach. Rapid Commun Mass Spectrom 26, 1347–1354. https://doi.org/10.1002/rcm.6231

Bengalli, R., Longhin, E., Marchetti, S., Proverbio, M.C., Battaglia, C., Camatini, M., 2017. The role of IL-6 released from pulmonary epithelial cells in diesel UFP-induced endothelial activation. Environ. Pollut. 231, 1314–1321. https://doi.org/10.1016/j.envpol.2017.08.104

Bengalli, R., Zerboni, A., Marchetti, S., Longhin, E., Priola, M., Camatini, M., Mantecca, P., 2019. In vitro pulmonary and vascular effects induced by different diesel exhaust particles. Toxicol. Lett. 306, 13–24. https://doi.org/10.1016/j.toxlet.2019.01.017

Bérubé, K., Prytherch, Z., Job, C., Hughes, T., 2010. Human primary bronchial lung cell constructs: the new respiratory models. Toxicology 278, 311–318. https://doi.org/10.1016/j.tox.2010.04.004

Bescond, A., Yon, J., Ouf, F.-X., Rozé, C., Coppalle, A., Parent, P., Ferry, D., Laffon, C., 2016. Soot optical properties determined by analyzing extinction spectra in the visible near-UV: Toward an optical speciation according to constituents and structure. Journal of Aerosol Science 101, 118–132. https://doi.org/10.1016/j.jaerosci.2016.08.001

Bhowmick, R., Gappa-Fahlenkamp, H., 2016. Cells and Culture Systems Used to Model the Small Airway Epithelium. Lung 194, 419–428. https://doi.org/10.1007/s00408-016-9875-2

Biswas, S.K., Rahman, I., 2009. Environmental toxicity, redox signaling and lung inflammation: The role of glutathione. Molecular Aspects of Medicine, Glutathione in Health and Disease 30, 60–76. https://doi.org/10.1016/j.mam.2008.07.001

Blank, F., Rothen-Rutishauser, B.M., Schurch, S., Gehr, P., 2006. An optimized in vitro model of the respiratory tract wall to study particle cell interactions. J Aerosol Med 19, 392–405. https://doi.org/10.1089/jam.2006.19.392

Boots, A.W., Gerloff, K., Bartholomé, R., van Berlo, D., Ledermann, K., Haenen, G.R.M.M., Bast, A., van Schooten, F.-J., Albrecht, C., Schins, R.P.F., 2012. Neutrophils augment LPS-mediated pro-inflammatory signaling in human lung epithelial cells. Biochim Biophys Acta 1823, 1151–1162. https://doi.org/10.1016/j.bbamcr.2012.04.012

Borgie, M., Dagher, Z., Ledoux, F., Verdin, A., Cazier, F., Martin, P., Hachimi, A., Shirali, P., Greige-Gerges, H., Courcot, D., 2015. Comparison between ultrafine and fine particulate matter collected in Lebanon: Chemical characterization, in vitro cytotoxic effects and metabolizing enzymes gene expression in human bronchial epithelial cells. Environmental Pollution 205, 250–260. https://doi.org/10.1016/j.envpol.2015.05.027

Chen, L., Deng, H., Cui, H., Fang, J., Zuo, Z., Deng, J., Li, Y., Wang, X., Zhao, L., 2017. Inflammatory responses and inflammation-associated diseases in organs. Oncotarget 9, 7204–7218. https://doi.org/10.18632/oncotarget.23208

Cho, H.-K., Park, C.-G., Shin, H.-J., Park, K.-H., Lim, H.-B., 2018. Comparison of the in vitro toxicological activity of various particulate matter. Toxicol Ind Health 34, 99–109. https://doi.org/10.1177/0748233717749694

Cho, H.-Y., Kleeberger, S.R., 2010. Nrf2 protects against airway disorders. Toxicol Appl Pharmacol 244, 43–56. https://doi.org/10.1016/j.taap.2009.07.024

Cui, Y., Chen, G., Yang, Z., 2020. Mitochondrial superoxide mediates PM2.5-induced cytotoxicity in human pulmonary lymphatic endothelial cells. Environmental Pollution 263, 114423. https://doi.org/10.1016/j.envpol.2020.114423

Daiber, A., Kuntic, M., Hahad, O., Delogu, L.G., Rohrbach, S., Di Lisa, F., Schulz, R., Münzel, T., 2020. Effects of air pollution particles (ultrafine and fine particulate matter) on mitochondrial function and oxidative stress – Implications for cardiovascular and neurodegenerative diseases. Archives of Biochemistry and Biophysics 696, 108662. https://doi.org/10.1016/j.abb.2020.108662

Dalle-Donne, I., Garavaglia, M.L., Colombo, G., Astori, E., Lionetti, M.C., La Porta, C.A.M., Santucci, A., Rossi, R., Giustarini, D., Milzani, A., 2020. Cigarette smoke and glutathione: Focus on in vitro cell models. Toxicol In Vitro 65, 104818. https://doi.org/10.1016/j.tiv.2020.104818

Dergham, M., Lepers, C., Verdin, A., Billet, S., Cazier, F., Courcot, D., Shirali, P., Garçon, G., 2012. Prooxidant and proinflammatory potency of air pollution particulate matter ($PM_{2.5-0.3}$) produced in rural, urban, or industrial surroundings in human bronchial epithelial cells (BEAS-2B). Chem Res Toxicol 25, 904–919. https://doi.org/10.1021/tx200529v

Fuentes-Mattei, E., Rivera, E., Gioda, A., Sanchez-Rivera, D., Roman-Velazquez, F.R., Jimenez-Velez, B.D., 2010. Use of human bronchial epithelial cells (BEAS-2B) to study immunological markers resulting from exposure to PM(2.5) organic extract from Puerto Rico. Toxicol Appl Pharmacol 243, 381–389. https://doi.org/10.1016/j.taap.2009.12.009

Fukai, T., Ushio-Fukai, M., 2011. Superoxide Dismutases: Role in Redox Signaling, Vascular Function, and Diseases. Antioxid Redox Signal 15, 1583–1606. https://doi.org/10.1089/ars.2011.3999

Harris, I.S., Treloar, A.E., Inoue, S., Sasaki, M., Gorrini, C., Lee, K.C., Yung, K.Y., Brenner, D., Knobbe-Thomsen, C.B., Cox, M.A., Elia, A., Berger, T., Cescon, D.W., Adeoye, A., Brüstle, A., Molyneux, S.D., Mason, J.M., Li, W.Y., Yamamoto, K., Wakeham, A., Berman, H.K., Khokha, R., Done, S.J., Kavanagh, T.J., Lam, C.-W., Mak, T.W., 2015.

Glutathione and Thioredoxin Antioxidant Pathways Synergize to Drive Cancer Initiation and Progression. Cancer Cell 27, 211–222. https://doi.org/10.1016/j.ccell.2014.11.019
Hawley, B., L'Orange, C., Olsen, D.B., Marchese, A.J., Volckens, J., 2014. Oxidative Stress and Aromatic Hydrocarbon Response of Human Bronchial Epithelial Cells Exposed to Petro- or Biodiesel Exhaust Treated with a Diesel Particulate Filter. Toxicol Sci 141, 505–514. https://doi.org/10.1093/toxsci/kfu147
Hernandez-Saavedra, D., Swain, K., Tuder, R., Petersen, S.V., Nozik-Grayck, E., 2017. Redox Regulation of the Superoxide Dismutases SOD3 and SOD2 in the Pulmonary Circulation, in: Wang, Y.-X. (Ed.), Pulmonary Vasculature Redox Signaling in Health and Disease, Advances in Experimental Medicine and Biology. Springer International Publishing, Cham, pp. 57–70. https://doi.org/10.1007/978-3-319-63245-2_5
Hsu, C.S., Lobodin, V.V., Rodgers, R.P., McKenna, A.M., Marshall, A.G., 2011. Compositional Boundaries for Fossil Hydrocarbons. Energy Fuels 25, 2174–2178. https://doi.org/10.1021/ef2004392
Hussar, E., Richards, S., Lin, Z.-Q., Dixon, R.P., Johnson, K.A., 2012. Human Health Risk Assessment of 16 Priority Polycyclic Aromatic Hydrocarbons in Soils of Chattanooga, Tennessee, USA. Water Air Soil Pollut 223, 5535–5548. https://doi.org/10.1007/s11270-012-1265-7
Jacobson, R.S., Korte, A.R., Vertes, A., Miller, J.H., 2020. The Molecular Composition of Soot. Angewandte Chemie International Edition 59, 4484–4490. https://doi.org/10.1002/anie.201914115
Juarez-Facio, A.T., Castilla, C., Corbière, C., Lavanant, H., Afonso, C., Morin, C., Merlet-Machour, N., Chevalier, L., Vaugeois, J.-M., Yon, J., Monteil, C., 2022. Development of a standardized in vitro approach to evaluate microphysical, chemical, and toxicological properties of combustion-derived fine and ultrafine particles. Journal of Environmental Sciences 113, 104–117. https://doi.org/10.1016/j.jes.2021.06.001
Kwon, H.-S., Ryu, M.H., Carlsten, C., 2020. Ultrafine particles: unique physicochemical properties relevant to health and disease. Exp Mol Med 52, 318–328. https://doi.org/10.1038/s12276-020-0405-1
Låg, M., Ovrevik, J., Refsnes, M., Holme, J., 2020. Potential role of polycyclic aromatic hydrocarbons in air pollution-induced non-malignant respiratory diseases. Respiratory Research 21. https://doi.org/10.1186/s12931-020-01563-1
Lavrich, K.S., Corteselli, E.M., Wages, P.A., Bromberg, P.A., Simmons, S.O., Gibbs-Flournoy, E.A., Samet, J.M., 2018. Investigating mitochondrial dysfunction in human lung cells exposed to redox-active PM components. Toxicology and Applied Pharmacology 342, 99–107. https://doi.org/10.1016/j.taap.2018.01.024
Leclercq, B., Kluza, J., Antherieu, S., Sotty, J., Alleman, L.Y., Perdrix, E., Loyens, A., Coddeville, P., Lo Guidice, J.-M., Marchetti, P., Garçon, G., 2018a. Air pollution-derived PM2.5 impairs mitochondrial function in healthy and chronic obstructive pulmonary diseased human bronchial epithelial cells. Environ. Pollut. 243, 1434–1449. https://doi.org/10.1016/j.envpol.2018.09.062
Leclercq, B., Kluza, J., Antherieu, S., Sotty, J., Alleman, L.Y., Perdrix, E., Loyens, A., Coddeville, P., Lo Guidice, J.-M., Marchetti, P., Garçon, G., 2018b. Air pollution-derived PM2.5 impairs mitochondrial function in healthy and chronic obstructive pulmonary diseased human bronchial epithelial cells. Environmental Pollution 243, 1434–1449. https://doi.org/10.1016/j.envpol.2018.09.062
Lee, W.-J., Wang, Y.-F., Lin, T.-C., Chen, Y.-Y., Lin, W.-C., Ku, C.-C., Cheng, J.-T., 1995. PAH characteristics in the ambient air of traffic-source. Science of The Total Environment 159, 185–200. https://doi.org/10.1016/0048-9697(95)04323-S
Li, N., Georas, S., Alexis, N., Fritz, P., Xia, T., Williams, M.A., Horner, E., Nel, A., 2016. A work group report on ultrafine particles (American Academy of Allergy, Asthma & Immunology): Why ambient ultrafine and engineered nanoparticles should receive

special attention for possible adverse health outcomes in human subjects. J. Allergy Clin. Immunol. 138, 386–396. https://doi.org/10.1016/j.jaci.2016.02.023
Li, N., Sioutas, C., Cho, A., Schmitz, D., Misra, C., Sempf, J., Wang, M., Oberley, T., Froines, J., Nel, A., 2003. Ultrafine particulate pollutants induce oxidative stress and mitochondrial damage. Environ. Health Perspect. 111, 455–460. https://doi.org/10.1289/ehp.6000
Liu, X., Meng, J., 2018. Tanshinone IIA ameliorates lipopolysaccharide-induced inflammatory response in bronchial epithelium cell line BEAS-2B by down-regulating miR-27a. Biomed Pharmacother 104, 158–164. https://doi.org/10.1016/j.biopha.2018.05.021
Livak, K.J., Schmittgen, T.D., 2001. Analysis of relative gene expression data using real-time quantitative PCR and the 2(-Delta Delta C(T)) Method. Methods 25, 402–408. https://doi.org/10.1006/meth.2001.1262
Longhin, E., Gualtieri, M., Capasso, L., Bengalli, R., Mollerup, S., Holme, J.A., Øvrevik, J., Casadei, S., Di Benedetto, C., Parenti, P., Camatini, M., 2016. Physico-chemical properties and biological effects of diesel and biomass particles. Environmental Pollution 215, 366–375. https://doi.org/10.1016/j.envpol.2016.05.015
Ma, Q., 2013. Role of Nrf2 in Oxidative Stress and Toxicity. Annu Rev Pharmacol Toxicol 53, 401–426. https://doi.org/10.1146/annurev-pharmtox-011112-140320
Mavin, E., Verdon, B., Carrie, S., Saint-Criq, V., Powell, J., Kuttruff, C.A., Ward, C., Garnett, J.P., Miwa, S., 2020. Real-time measurement of cellular bioenergetics in fully differentiated human nasal epithelial cells grown at air-liquid-interface. Am J Physiol Lung Cell Mol Physiol 318, L1158–L1164. https://doi.org/10.1152/ajplung.00414.2019
Mistry, A., Bowen, L.E., Dzierlenga, M.W., Hartman, J.K., Slattery, S.D., 2020. Development of an in vitro approach to point-of-contact inhalation toxicity testing of volatile compounds, using organotypic culture and air-liquid interface exposure. Toxicology in Vitro 69, 104968. https://doi.org/10.1016/j.tiv.2020.104968
Moorthy, B., Chu, C., Carlin, D.J., 2015. Polycyclic aromatic hydrocarbons: from metabolism to lung cancer. Toxicol. Sci. 145, 5–15. https://doi.org/10.1093/toxsci/kfv040
Nebert, D.W., Dalton, T.P., Okey, A.B., Gonzalez, F.J., 2004. Role of Aryl Hydrocarbon Receptor-mediated Induction of the CYP1 Enzymes in Environmental Toxicity and Cancer*. Journal of Biological Chemistry 279, 23847–23850. https://doi.org/10.1074/jbc.R400004200
Oberdörster, G., Oberdörster, E., Oberdörster, J., 2005. Nanotoxicology: an emerging discipline evolving from studies of ultrafine particles. Environ. Health Perspect. 113, 823–839. https://doi.org/10.1289/ehp.7339
Ohura, T., Amagai, T., Fusaya, M., Matsushita, H., 2004. Polycyclic Aromatic Hydrocarbons in Indoor and Outdoor Environments and Factors Affecting Their Concentrations. Environ. Sci. Technol. 38, 77–83. https://doi.org/10.1021/es030512o
Palma, F.R., He, C., Danes, J.M., Paviani, V., Coelho, D.R., Gantner, B.N., Bonini, M.G., 2020. Mitochondrial Superoxide Dismutase: What the Established, the Intriguing, and the Novel Reveal About a Key Cellular Redox Switch. Antioxid Redox Signal 32, 701–714. https://doi.org/10.1089/ars.2019.7962
Penn, A., Murphy, G., Barker, S., Henk, W., Penn, L., 2005. Combustion-Derived Ultrafine Particles Transport Organic Toxicants to Target Respiratory Cells. Environ Health Perspect 113, 956–963. https://doi.org/10.1289/ehp.7661
Pope, C.A., Dockery, D.W., 2006. Health effects of fine particulate air pollution: lines that connect. J Air Waste Manag Assoc 56, 709–742. https://doi.org/10.1080/10473289.2006.10464485
Ricciardolo, F.L.M., Sorbello, V., Benedetto, S., Defilippi, I., Sabatini, F., Robotti, A., van Renswouw, D.C., Bucca, C., Folkerts, G., De Rose, V., 2012. Bradykinin- and lipopolysaccharide-induced bradykinin B2 receptor expression, interleukin 8 release

and “nitrosative stress” in bronchial epithelial cells BEAS-2B: role for neutrophils. Eur J Pharmacol 694, 30–38. https://doi.org/10.1016/j.ejphar.2012.07.051
Rubio, V., Zhang, J., Valverde, M., Rojas, E., Shi, Z.-Z., 2011. Essential role of Nrf2 in protection against hydroquinone- and benzoquinone-induced cytotoxicity. Toxicol In Vitro 25, 521–529. https://doi.org/10.1016/j.tiv.2010.10.021
Siegmann, K., Hepp, H., Sattler, K., 1995. Reactive Dimerization: A New PAH Growth Mechanism in Flames. Combustion Science and Technology 109, 165–181. https://doi.org/10.1080/00102209508951900
Siegmann, K., Sattler, K., 1999. Formation mechanism for polycyclic aromatic hydrocarbons in methane flames. J. Chem. Phys. 112, 698–709. https://doi.org/10.1063/1.480648
Sies, H., Jones, D., 2007. Oxidative Stress*, in: Fink, G. (Ed.), Encyclopedia of Stress (Second Edition). Academic Press, New York, pp. 45–48. https://doi.org/10.1016/B978-012373947-6.00285-3
Sotty, J., Kluza, J., De Sousa, C., Tardivel, M., Anthérieu, S., Alleman, L.-Y., Canivet, L., Perdrix, E., Loyens, A., Marchetti, P., Lo Guidice, J.-M., Garçon, G., 2020a. Mitochondrial alterations triggered by repeated exposure to fine (PM2.5-0.18) and quasi-ultrafine (PM0.18) fractions of ambient particulate matter. Environment International 142, 105830. https://doi.org/10.1016/j.envint.2020.105830
Sotty, J., Kluza, J., De Sousa, C., Tardivel, M., Anthérieu, S., Alleman, L.-Y., Canivet, L., Perdrix, E., Loyens, A., Marchetti, P., Lo Guidice, J.-M., Garçon, G., 2020b. Mitochondrial alterations triggered by repeated exposure to fine (PM2.5-0.18) and quasi-ultrafine (PM0.18) fractions of ambient particulate matter. Environ Int 142, 105830. https://doi.org/10.1016/j.envint.2020.105830
Stewart, C.E., Torr, E.E., Mohd Jamili, N.H., Bosquillon, C., Sayers, I., 2012. Evaluation of Differentiated Human Bronchial Epithelial Cell Culture Systems for Asthma Research. J Allergy (Cairo) 2012. https://doi.org/10.1155/2012/943982
Totlandsdal, A.I., Herseth, J.I., Bølling, A.K., Kubátová, A., Braun, A., Cochran, R.E., Refsnes, M., Ovrevik, J., Låg, M., 2012. Differential effects of the particle core and organic extract of diesel exhaust particles. Toxicol Lett 208, 262–268. https://doi.org/10.1016/j.toxlet.2011.10.025
Totlandsdal, A.I., Låg, M., Lilleaas, E., Cassee, F., Schwarze, P., 2015. Differential proinflammatory responses induced by diesel exhaust particles with contrasting PAH and metal content. Environ Toxicol 30, 188–196. https://doi.org/10.1002/tox.21884
Uppstad, H., Øvrebø, S., Haugen, A., Mollerup, S., 2010. Importance of CYP1A1 and CYP1B1 in bioactivation of benzo[a]pyrene in human lung cell lines. Toxicol Lett 192, 221–228. https://doi.org/10.1016/j.toxlet.2009.10.025
Walgraeve, C., Demeestere, K., Dewulf, J., Zimmermann, R., Van Langenhove, H., 2010. Oxygenated polycyclic aromatic hydrocarbons in atmospheric particulate matter: Molecular characterization and occurrence. Atmospheric Environment 44, 1831–1846. https://doi.org/10.1016/j.atmosenv.2009.12.004
Wang, Y., Tang, M., 2018. Review of in vitro toxicological research of quantum dot and potentially involved mechanisms. Science of The Total Environment 625, 940–962. https://doi.org/10.1016/j.scitotenv.2017.12.334
Xin, R., Pan, Y.-L., Wang, Y., Wang, S.-Y., Wang, R., Xia, B., Qin, R.-N., Fu, Y., Wu, Y.-H., 2019. Nickel-refining fumes induce NLRP3 activation dependent on mitochondrial damage and ROS production in Beas-2B cells. Arch Biochem Biophys 676, 108148. https://doi.org/10.1016/j.abb.2019.108148

Hybrid catalyst cascade for enhanced oxidation of glucose in glucose/air biofuel cell

Gangyong Li [a,b], Zongdong Wu [b], Cuixing Xu [b,c], Zongqian Hu [b,*]

a. State Key Laboratory of Advanced Metallurgy, University of Science and Technology Beijing, Beijing 100083, China

b. Beijing Institute of Radiation Medicine, Beijing 100850, China

c. Key Laboratory of Polyoxometalate and Reticular Material Chemistry of Ministry of Education, National & Local United Engineering Laboratory for Power Batteries, Key Laboratory of Nanobiosensing and Nanobioanalysis at Universities of Jilin Province, Analysis and Testing Center, Department of Chemistry, Northeast Normal University, Changchun, Jilin Province, 130024, China

** Corresponding author, Email: huzongqian@hotmail.com*

Abstract

Redox enzymes are capable of harvesting electrical energy from biofuels in high catalytic activity and under mild condition. However, it is difficult to achieve efficient electron transfer and deep oxidation of biofuels simultaneously in a single-enzyme catalytic system. Herein, we report a hybrid catalyst cascade consisting of an organic oxidation catalyst, 2,2,6,6-tetramethyl-1-piperidine N-oxyl (TEMPO), and an enzyme, glucose oxidase (GOx), for electrochemical oxidation of glucose. It is found that TEMPO is capable of mediating electron transfer between the redox center of GOx and the electrode surface. While glucose can be oxidized into glucuronic acid under neutral conditions. Thus, combining GOx and TEMPO, we are able to achieve $4e^-$ electrooxidation of glucose using the hybrid enzymatic and organic cascade (HEOC) system. When coupled with an air-breathing Pt cathode, the resulting glucose/air biofuel cell using the proposed HEOC anode exhibits a maximum power density of 38.1 $\mu W\ cm^{-2}$ with a short-circuit current of 651.4 $\mu A\ cm^{-2}$, which can be attributed to the enhanced energetic efficiency, enabling TEMPO a promising catalyst for glucose oxidation in bioelectronics applications.

Keywords: glucose, organic catalyst, glucose oxidase, cascade catalysis, enzymatic biofuel cell

1. Introduction

Glucose is a promising fuel because it is abundant in nature, renewable, safe for storage and distribution, non-toxic, and inexpensive, and has relatively high energy density [1,2]. One option for the energy conversion of glucose into electricity is fuel cells (FCs). However, the widespread use of precious metal-catalyzed FCs raises concerns about the availability of costly, limited, irreplaceable metal resources [3-7]. In addition, these catalysts often require alkaline conditions and elevated temperature to achieve an increased oxidation rate [8]. Enzymatic biofuel cells (EBFCs) employing redox enzymes to catalyze the oxidation of a fuel at the bioanode or the reduction of an oxidant at the biocathode, are capable of directly converting chemical energy from biofuels into electricity by means of the catalytic activity of enzymes under mild conditions (ambient temperature and neutral pH) [9,10]. Additionally, using biocatalysts, EBFCs have advantages of renewable catalyst and fuel diversity.

Collecting electrons produced in the bioelectrocatalytic reaction between redox enzymes and their substrates at an electrode surface is a key element of EBFCs. In some case, enzymes are able to undergo direct electron transfer (DET) with an electrode surface [11,12]. However, DET requires strict orientation of enzyme molecules and the electrode surface can only be simultaneously connected to a maximum of a single layer of enzymes [13]. In most case, DET between the enzyme and the electrode is quite difficult because of the large size and spatial structure of the enzymes [10]. Especially, when the redox active center of enzymes is deeply buried within the insulating protein [14]. Therefore, small electroactive molecules are

utilized as redox mediators to shuttle electrons between the enzyme cofactor and the electrode surface, which is called mediated electron transfer (MET) [15,16]. For instance, ferrocene-based compounds [17-19], tetrathiafulvalene [20], 1,4-naphthoquinone [21], 1-methoxy-5-methylphenazinium methylsulfate [22], methylene blue [23, 24], and 1,4-benzoquinone [25], et al. are commonly used as redox mediators to shuttle electrons for the anodic oxidation of biofuels. Unfortunately, these mediators are incapable of oxidizing glucose (**Fig. S1**). In a single anodic enzymatic catalytic system, there is only $2e^-$ transfer during the oxidation process, which reserves the majority of energy within the oxidation products of glucose [26]. Therefore, exploiting novel electron mediators capable of catalyzing oxidation of glucose is interesting and is of significance in the development of glucose EBFCs.

TEMPO (2,2,6,6-tetramethyl-1-piperidine N-oxyl) and its derivatives are important organic oxidation catalysts for the oxidation of a wide range of alcohols and aldehydes at room temperature and under mild aqueous conditions in industrial and laboratory applications [27,28], these merits make it attractive in FC application [8,26,29-31]. Herein, we describe a novel hybrid enzymatic and organic cascade (HEOC) system consisting of glucose oxidase (GOx) and TEMPO for enhanced glucose oxidation. Interestingly, electrochemical measurements reveal that TEMPO can not only function as an electrocatalyst to catalyze $4e^-$ oxidation of glucose under neutral condition, but also serve as a redox mediator to shuttle electrons between GOx and the electrode surface, therefore, the energetic efficiency of this cascade catalysis

is significantly enhanced. Consequently, the constructed glucose/air EBFCs using the HEOC anode and an air-breathing Pt cathode deliver a maximum power density of 38.1 μW cm^{-2}, with a short-circuit current of 651.4 μA cm^{-2}. The proposed strategy could be used to fabricate novel energy conversion system with high efficiency for a wide range of substrates such as sugar and alcohol.

2. Experimental

2.1. Materials and reagents

All reagents were of analytical grade and obtained from commercial sources and used without further purification. GOx (200 U mg^{-1} solid, from *Aspergillus niger*) and Nafion 117 membrane were purchased from Alfa-Aesar. TEMPO, D-gluconolactone, glucuronic acid, Nafion solution (5%), and Pt/C catalyst (10 wt.%) were purchased from Sigma-Aldrich. Flavin adenine dinucleotide (FAD)-dependent glucose dehydrogenase (GDH, 1170 U mg^{-1}, from *Aspergillus sp.*) was purchased from Sekisui Diagnostics (UK). Bovine serum albumin (BSA, 96%) and polytetrafluoroethylene (PTFE) dispersion (60 wt%) were obtained from Aladdin. Milli-Q ultrapure water (18.2 MΩ cm) was used throughout the experiments and all experiments were performed under room temperature.

2.2. Preparation of working electrodes

N-doped reduced graphene oxide@carbon nanotubes (N-RGO@CNTs) nanocomposite utilized as supporting material to immobilize GOx, GDH, and BSA on glassy carbon electrode (GCE, 3 mm in diameter) was synthesized according to our

previous work [32]. For the fabrication of GOx-modified working electrodes, 20 μL of N-RGO@CNTs dispersion (10 mg mL^{-1} in ultrapure water) was mixed with 20 μL of GOx solution (30 mg mL^{-1} in 0.1 M PBS at pH 7.0) by vortexing. 5 μL of the mixture was then casted on the surface of the polished GCE. After drying in a refrigerator at 4 °C, 5 μL of Nafion solution (0.5%) was casted on the surface of the GOx/N-RGO@CNTs modified-GCE and the electrodes were stored in refrigerator at 4 °C before use. As contrast, BSA- and GDH-modified electrodes were prepared in the similar procedure.

2.3 Preparation of air-breathing Pt cathode

The air-breathing Pt cathode was a Toray carbon cloth coated with a Pt/C catalyst layer on one side and a PTFE diffusion layer coated on the other side. Typically, 100 μL of 60 wt% PTFE solution was coated onto one side of a carbon cloth and allowed the coating layer to air-dry. The dried carbon cloth was placed on a ceramic plate in a pre-heated furnace at 370 ºC for 20 min to form the PTFE diffusion layer. For the construction of Pt/C catalyst layer, 10 mg of 10 wt% Pt/C was dispersed in a mixture of Nafion 117 solution (100 μL), deionized water (700 μL), and iso-propanol (200 μL). 20 μL of the mixture was then coated onto the carbon side (6 mm in diameter) opposite the PTFE diffusion layer and dried at room temperature.

2.4. Electrochemical measurements

The electrocatalytic oxidation of glucose by TEMPO was characterized in 0.1 M PBS (pH 7.0) by cyclic voltammetry (CV) using a typical three-electrode system with an Ag/AgCl (saturated KCl) as the reference electrode, Pt foil (1 cm^2) as the counter

electrode, and a GCE as the working electrode. 0.1 M PBS (pH 7.0) containing 1 mM TEMPO in the presence and absence of 50 mM glucose was used as the electrolyte.

The hybrid enzymatic and organic electrocatalytic oxidation of glucose was carried out by CV and chronoamperometric (CA) measurements. The CVs were recorded in N_2-saturated 0.1 M PBS (pH 7.0) containing 1 mM TEMPO in the presence and absence of 50 mM glucose. The CA measurements were performed at an applied potential of 0.5 V (vs. Ag/AgCl) on successive addition of glucose into N_2-saturated 0.1 M PBS (pH 7.0). Bulk electrolysis experiment was performed in 0.1 M PBS at pH 7.0 with an Ag/AgCl (saturated KCl) as the reference electrode, Pt foil (1 cm^2) as the counter electrode, and a GOx/N-RGO@CNTs modified GCE as the working electrode at an applied bias of 0.5 V (vs. Ag/AgCl). The oxidation products were quantified by mass spectrometry (MS), which was operated on a Thermo Fisher Scientific LTQ FT Utra (ESI) mass spectrometer.

2.5. Biofuel cell measurements

EBFCs were tested using one-chamber cell where the anode was GOx/N-RGO@CNTs modified GCE immersed in N_2-saturated 0.1 M PBS at pH 7.0 containing 50 mM glucose and 1 mM TEMPO. The cathode was a Toray carbon cloth coated with a Pt/C catalyst layer on one side and a PTFE diffusion layer on the other side. The separator was a Nafion 117 membrane. The cell was operated in quiescent condition with pure O_2 flowing in the cathode chamber. Linear sweep voltammetry (LSV) was performed at 1.0 mV s^{-1} from the open circuit voltage of the cell to 0 V to evaluate the performance of the BFCs. The output density and current density were